

# Massive Spatial Qubits for Testing Macroscopic Nonclassicality and Casimir Induced Entanglement

Bin Yi,<sup>1</sup> Urbasi Sinha,<sup>2</sup> Dipankar Home,<sup>3</sup> Anupam Mazumdar,<sup>4,5</sup> and Sougato Bose<sup>1</sup>

<sup>1</sup>*Department of Physics and Astronomy, University College London, Gower Street, WC1E 6BT London, United Kingdom.*

<sup>2</sup>*Raman Research Institute, C. V. Raman Avenue, Sadashivanagar, Bengaluru, Karnataka 560080, India*

<sup>3</sup>*Center for Astroparticle Physics and Space Science (CAPSS), Bose Institute, Kolkata 700 091, India*

<sup>4</sup>*University of Groningen, PO Box 72, 9700 Groningen, Netherlands*

<sup>5</sup>*Van Swinderen Institute, University of Groningen, 9747 AG Groningen, Netherlands*

(Dated: May 29, 2022)

## Abstract

An open challenge in physics is to expand the frontiers of the validity of quantum mechanics by evidencing nonclassicality of the centre of mass state of a macroscopic object. Yet another equally important task is to evidence the essential nonclassicality of the interactions which act between macroscopic objects. Here we introduce a new tool to meet these challenges: massive spatial qubits. In particular, we show that if two distinct localized states of a mass are used as the  $|0\rangle$  and  $|1\rangle$  states of a qubit, then we can measure this encoded spatial qubit with a high fidelity in the  $\sigma_x$ ,  $\sigma_y$  and  $\sigma_z$  bases simply by measuring its position after different durations of free evolution. We show how this technique can be used to reveal an irreducible nonclassicality through a Bell-inequality violation arising from the entanglement of the centre of mass of a nano-crystal with its spin in a Stern-Gerlach setup. Secondly, we show how our methodology, in conjunction with the Casimir interaction, offers a powerful method to create and certify non-Gaussian entanglement between two neutral nano-objects. Fundamentally, the generation of such an entanglement provides an empirical means for demonstrating an inherent quantumness of the Casimir interaction.

*Introduction.* It is an open challenge to evidence nonclassicality in the behaviour of the centre of mass of a massive object, and thereby extend the boundaries of the validity of quantum mechanics [1, 2]. To date, the state of art demonstrations of nonclassicality have only reached up to macromolecules of  $10^4$  amu mass [3, 4]. It is thus pivotally important to observe nonclassical behaviour with ever more massive objects, for which, while there are many ideas to date [5–12], implementations are yet to come. If no speculated modifications of quantum mechanics [13–18] are found on the way, and enough environmental isolation can be successfully achieved, then such nonclassicalities would open varied avenues. This includes foundational applications, such as testing the quantum character of gravity [19–23], as well as practical applications in the quantum sensing of acceleration and classical gravity [24]. Identifying new tools to probe this question of macroscopic nonclassicality (by which here we mean in terms of large mass) is thus particularly important. Motivated by this, here we propose and examine the efficacy of precisely such a tool: a mechanism to read out a qubit encoded in the spatial degree of freedom of a *free (untrapped) mass* (a purely spatial qubit). A principal merit of this scheme is its simplicity: *measuring* the spatial qubit operators  $\sigma_x$ ,  $\sigma_y$  and  $\sigma_z$  exploits solely the free time evolution of the mass (Hamiltonian  $H = \hat{p}^2/2m$ ), followed by the detection of its position. As the mass is not controlled/trapped by any fields during the free evolution part of this measurement, there is no decoherence induced by such processes. This is obviously a generic enabler of qubit based technologies applicable for any mass (including, for example, electrons, neutrons and atoms). However, here we are going to focus on larger masses in view of the foundational significance mentioned above.

As a first application, we show that our tool enables the verification of an irreducible nonclassicality of a particular joint state of a spin (a well established quantum degree spin) and the centre of mass of a macroscopic object, whose quantum nature is yet to be established. To this end, we use the state produced in a Stern-Gerlach apparatus which is usually written down as a quantum *entangled* state of a spin and the position [22, 25–28]. Such Stern-Gerlach states have been created with atoms and the coherence of the spatial part alone has been verified by interferometry after selecting a specific spin state [28, 29], the so called *spatial fringe interferometer*. An alternative is to verify the coherence by undoing the Stern-Gerlach splitting – so called “closing the loop” [27], which, while it may scale to large masses in the future [22, 30], is extremely difficult [22, 25]. However, there are, as yet, no protocols to verify the *entanglement* between the spin of an object in a Stern-Gerlach

experiment and the motion of its centre of mass in a way which can be scaled to macroscopic objects. We show that this can be accomplished via the violation of a Bell’s inequality in which the spin and the positions of the mass are measured. This violation will also prove the nonclassicality of a large mass in terms of quantum contextuality [31, 32]. The degree of this violation can also be used to estimate the decoherence of this mass from its interaction with its the environment, as well as from any fundamental modifications of quantum mechanics. In this aspect it also has some advantages: it can be used to test decoherence of the mass in multiple bases in the *same* experiment [33] (in a manner which will be clarified later) and does not rely on inducing special types of cyclic entanglement-disentanglement dynamics of the mass with an ancillary system as in some previous schemes for observing macroscopic decoherence [5–8].

Next, we propose a second application once the quantum nature of the centre of mass degree of freedom of macroscopic objects is assumed (or established in the above, or in some other way). This application has import in establishing the quantum nature of the interactions between macroscopic objects. We show how our spatial qubit methodology can enable witnessing the entanglement created between two neutral nano-crystal masses through their Casimir interaction (a minor additional squeezing operation has to be appended). This has two types of foundational imports: (a) It shows that the Casimir interaction has a quantum origin – it is mediated by virtual photons – the quantum nature of these is the cause of entanglement between the masses (if the agent going between the masses was classical it would not entangle [19–21, 34, 35]; for example, qubits get entangled when they interact electromagnetically i.e., exchange of virtual photons, is well established in experiments [36, 37] – if the virtual photons were replaced by classical entities they would not entangle). Though there have been numerous experiments on Casimir interactions [38], only recently these have proceeded to the nano-scale. For example, they have been exploited for torques on nanocrystals [39], and for transferring energy between two microstructures [40]. However, their ability to generate quantum entanglement has not yet been established, which our proposal can fulfill. (b) As the entangled state is generated by starting from superpositions of distinct localized (Gaussian) states, it is highly non-Gaussian in nature, and will be a unique example of how to generate and *verify* such a state for two nano-crystals (mass  $\sim 10^{-19}$  kg). While there are some ideas to date for the generation of Gaussian entangled states of nano-scale masses (e.g., [41–43]) where the familiar EPR criterion [44] to witness entanglement can be applied,

there are hardly any schemes to either generate or witness non-Gaussian entangled states of nano-crystals. The realization of a Casimir induced entanglement of the above form will thus be complementary to most work in the entanglement frontier of nano-crystals, which are in the Gaussian regime.

We are achieving our tool by combining ideas from two different quantum technologies together: photonic quantum information processing and the trapping, cooling and manipulation of micro-crystals. In the former field it is known that a qubit can be encoded in the spatial mode of a single photon by passing it through an effective Young's double slit [45]. These qubits, called Young qubits, and their qudit (quantum d-level system) counterparts [46, 47], have been exploited to perform certain quantum information processes [48, 49]. However, this useful encoding has not yet been adapted to other quantum technologies. On the other hand, we have had a rapid development recently in the field of levitated quantum objects – namely nano and micro-crystals, starting with theoretical ideas [9, 10, 50] and culminating in recent cooling to the ground state and verification of energy quantization [51, 52]. While several schemes for verifying quantum superpositions of distinct states of such objects have been proposed to date, in these schemes, either the  $x$ ,  $y$  and  $z$  motions are measured as infinite dimensional quantum systems [12, 53, 54] rather than being discretized as an effective qubit, or never measured at all (only ancillary systems coupled to them, such as spins are measured [30, 55]). Adapting the idea of Young qudits from photonic technologies, we show here how to make them applicable to massive systems. Note that the idea of encoding a qubit in a continuous variable system was first proposed as a quantum error correction code [56], although that uses a very different encoding, and uses a harmonic oscillator system rather than a free particle, which is not ideal in our large mass context as any trapping mechanism itself causes decoherence. While our focus in this paper is to show how well Young qubits facilitate the probing of the macroscopic limits of quantum mechanics and testing the quantum nature of an unavoidable interaction between neutral macroscopic objects (i.e., the Casimir interaction), it is quite possible that this spatial qubit encoding and measurements may be applied to lower mass (less decohering) neutral objects such as atoms in free flight, as qubits in quantum information processing.

*Qubit Encoding and its Measurement in all Bases:* We encode the qubit in the spatial mode of a single massive object. The encoding is very intuitive, the  $|0\rangle$  and  $|1\rangle$  states of a qubit are represented by two spatially separated (say, in the  $x$  direction) non-overlapping

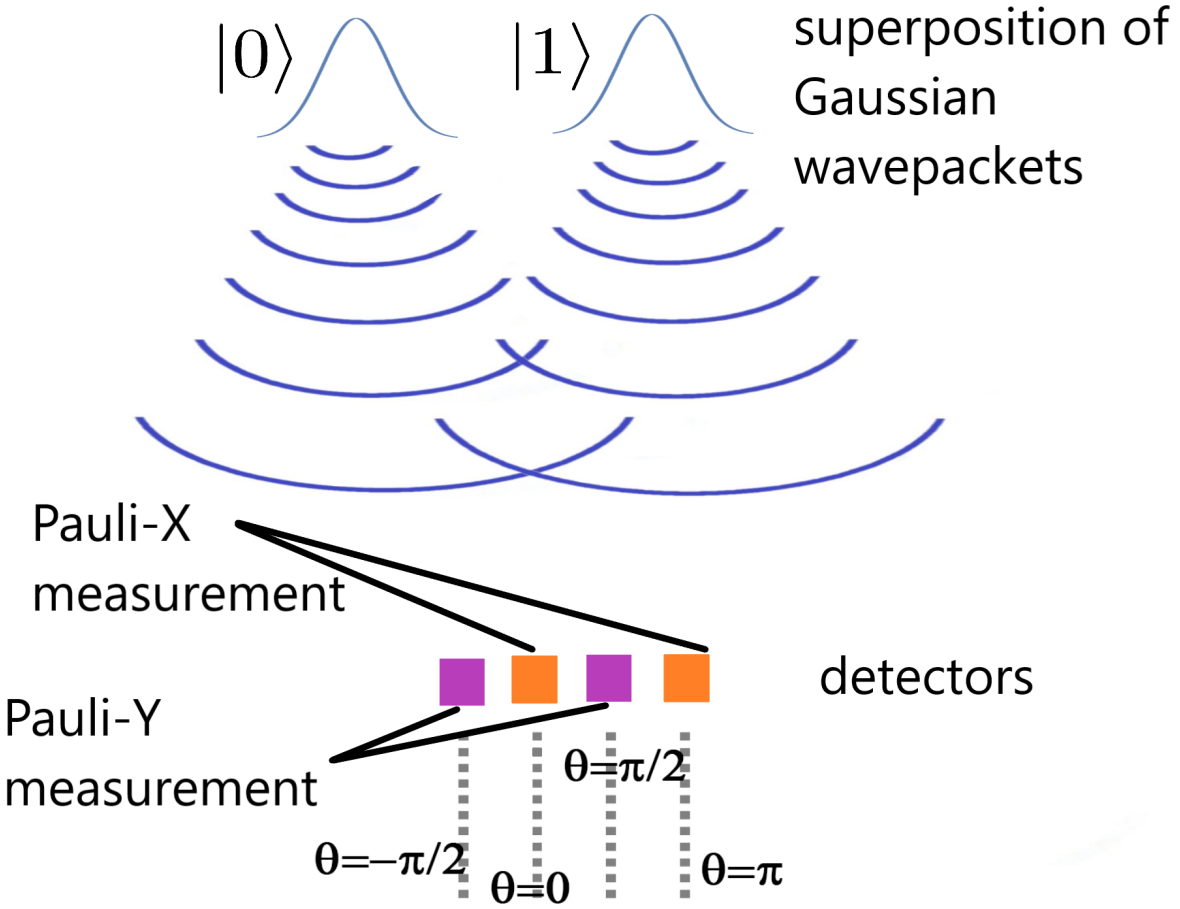


FIG. 1. **Spatial detection as Pauli-x, Pauli-y measurements:** a pair of detectors (color: orange) located at phase angle  $\theta = 0, \theta = \pi$  perform Pauli-x measurement. The detectors (color: purple) at  $\theta = \pi/2, \theta = -\pi/2$  perform of Pauli-y measurement.

wavepackets whose position and momenta are both centred around zero in the other two commuting ( $y$  and  $z$ ) directions. Explicitly, these states (writing only the  $x$  part of their wavefunction) are

$$|0\rangle = \frac{1}{\sqrt{\sigma_d \pi^{1/4}}} \int_{-\infty}^{\infty} \exp\left[-\frac{(x + d/2)^2}{4\sigma_d^2}\right] |x\rangle dx \quad (1)$$

$$|1\rangle = \frac{1}{\sqrt{\sigma_d \pi^{1/4}}} \int_{-\infty}^{\infty} \exp\left[-\frac{(x - d/2)^2}{4\sigma_d^2}\right] |x\rangle dx \quad (2)$$

with  $d \gg \sigma_d$ . These states are schematically depicted in Fig. 1 in which only the  $x$  direction is depicted along with their evolution in *time*, which will be important later. For simplicity of presentation, we will omit the acceleration due to the Earth's gravity, which is a part of the evolution which commutes with the rest (just imagine the experiment taking place in

a freely falling frame – everything can be easily adjusted to incorporate the acceleration). Under the above omission, the time evolution of our qubit state, which is essentially what we will exploit in this paper, maintains a complete cylindrical symmetry about the  $x$  axis. Thus effectively we only consider 1D evolution in the  $x$  direction.

In this paper, we will only require two classes of states: (a) a state in which a spin embedded in a mass is entangled with the mass’s spatial degree of freedom in the state  $|\phi^+\rangle = \frac{1}{\sqrt{2}}(|\uparrow, 1\rangle + |\downarrow, 0\rangle)$  for our first application, and (b) the spatial qubit state  $|+\rangle = \frac{1}{\sqrt{2}}(|0\rangle + |1\rangle)$  as a resource for our second application. Preparation of the above follows/combines previous proposals and will be discussed along with the respective applications. Here we just mention that the state  $|\phi^+\rangle = \frac{1}{\sqrt{2}}(|\uparrow, 1\rangle + |\downarrow, 0\rangle)$  we can use the so called *half-loop* of a Stern-Gerlach interferometry [28, 29] (in which  $|\uparrow\rangle$  makes centre of mass accelerate right and  $|\downarrow\rangle$  makes centre of mass accelerate left, are decelerated by appropriate fields for an appropriate time to become separated spatial qubit states  $|1\rangle$  and  $|0\rangle$  respectively). The preparation of the state  $|+\rangle$  can follow from  $|\phi^+\rangle$  by “sub-selecting” only one of the spin states after an appropriate microwave pulse superposes the spin states, as in the *spatial fringe interferometer* described in Refs.[28, 29]. Alternatively, a Stern-Gerlach half loop can also be followed by a spatial qubit-spin disentangling operation by suitable microwave pulses on the spin as discussed in Ref.[54] to also create  $|+\rangle$  of a nanocrystal. Another alternative can be to prepare a nanocrystal directly in a  $|+\rangle$  state by an effective measurement on the mass via a cavity field [12].

We now outline the way and efficacy of measuring the above encoded spatial qubit in various bases, which is our central tool. Projective measurement on the qubit can be performed by detecting the mass at certain positions. This will be done by measuring the position of the mass by scattering light from it, which is an extremely efficient method with extremely high spatial resolution [57, 58] – unlike the case of photons or small mass objects such as electrons and atoms, here there are no issues of either missing a freely moving micro-object when enough light is shone on it (i.e., particle losses) or falsely registering an object when there is none (i.e., dark counts). Note that due to the spreading of wavepackets along  $y$  and  $z$  directions as well, when we determine whether the object is in a given position  $x = x_0$  at some measurement time  $t$ , we are essentially integrating the probability of detecting it over a finite region  $\Delta y(t)$  and  $\Delta z(t)$  which takes into account the wavepacket spread of the massive object in the  $y$  and  $z$  directions at time  $t$ . The operator  $\sigma_z = |0\rangle\langle 0| - |1\rangle\langle 1|$

is the trivial one to measure, as we simply shine a laser centred at  $x = d/2$  and a beam waist  $\ll d$  much before the wavepacket states  $|0\rangle$  and  $|1\rangle$  have started to overlap (at a time  $t_{\text{meas}}^z \ll d(2\sigma_d m)/\hbar$ ; the error in  $\sigma_z$  measurement as a function of the time  $t_{\text{meas}}^z$  is described in the appendix; timing errors  $\delta t \ll t_{\text{meas}}^z$  have very little effect on the error in  $\sigma_z$  measurement). If light is scattered, the state is  $|0\rangle$ , otherwise  $|1\rangle$ .

To measure the spatial qubit  $\sigma_x$  and  $\sigma_y$  operators, we need a large enough time  $t_{\text{meas}}^{x,y} \geq d(2\sigma_d m)/\hbar$  so that the wavepackets corresponding to the states  $|0\rangle$  and  $|1\rangle$  have spread out enough to significantly overlap with each other and an interference pattern that involves the relative phase between  $|0\rangle$  and  $|1\rangle$  is produced. Moreover, due to the free propagation of the wavepackets, we would expect the measurement time  $t_{\text{meas}}^{x,y}$ , final position  $x$  and the transverse wave vector  $k_x$  are related by:  $x = \frac{\hbar k_x t_{\text{meas}}^{x,y}}{m}$  (detecting at a position  $x$  after the interference effectively measures the initial superposition state of  $|0\rangle$  and  $|1\rangle$  in the  $|k_x\rangle$  basis). Noting the momentum representation of the qubit states

$$|n\rangle = \int \left\{ \sqrt{2}\sigma_d \exp\left[\frac{ik_x d}{2} - k_x^2 \sigma_d^2\right] \exp[-ink_x d] |k_x\rangle \right\} dk_x \quad (3)$$

where  $n = 0, 1$ , the probability to detect the object at a position  $x$  for any initial qubit state  $|\psi\rangle$  is then given by

$$P(x) = |\langle\psi|k_x\rangle|^2 \propto \left| \exp\left[\frac{ik_x d}{2} - k_x^2 \sigma_d^2\right] \langle\theta|\psi\rangle \right|^2 \quad (4)$$

where  $|\theta\rangle = |0\rangle + |1\rangle e^{i\theta}$  in which the parameter  $\theta = k_x d = \frac{xmd}{\hbar t_{\text{meas}}^{x,y}}$  (we will call  $\theta$  the phase angle). Therefore, finding the object in various positions  $x$  is in one to one correspondence with positive operator valued measurements (POVM) on the spatial qubit, with the relevant projection on the state being, up to a normalization factor, as  $|\theta\rangle\langle\theta|$ . The  $\sigma_x$  ( $\sigma_y$ ) measurements can therefore be implemented by placing a pair of position detectors (which will, in practice be, lasers scattering from the object) at positions corresponding to phase angle  $\theta = 0, \theta = \pi, \theta = \pi/2, \theta = -\pi/2$  respectively (Schematic diagram shown in Fig1). For minimizing the time of the experiment, we are going to choose  $t_{\text{meas}}^{x,y} = d(2\sigma_d m)/\hbar$ . The efficacy of the  $\sigma_x$  and  $\sigma_y$  measurements as a function of the finite time  $t_{\text{meas}}^{x,y}$  for various ratios  $\sigma_d : d$  is discussed in the appendix.

*Nonclassicality of the Stern-Gerlach state:* As a first application of this spatial qubit technology, we consider an extra spin degree of freedom embedded in a mesoscopic mass. We now imagine that the mass goes through a Stern-Gerlach apparatus. The motion of

the mass relative to the source of the inhomogeneous magnetic field (current/magnets) is affected in a spin dependent manner due to the exchange virtual photons between the source and the spin. This quantum field theoretic process is depicted in the inset of Fig.2 <sup>1</sup>. The result is an entangled state of the spin and position of the nano-object as given by  $|\phi^+\rangle = \frac{1}{\sqrt{2}}(|\uparrow, 1\rangle + |\downarrow, 0\rangle)$ , as depicted as the output of the preparation stage in Fig.2. This type of entanglement can be regarded as a micro-macro entanglement as a microscopic system (spin) and a macroscopic system (the centre of mass degree of freedom of a nanocrystal), similar to its previous usage in the context of two modes of light [59] and light and an atomic ensemble [60]. It could also be regarded as an intra-particle entanglement (an entanglement between two degrees of freedom of the same object), which has also been a subject of several investigations [31, 61]. However those techniques are not readily adaptable to massive objects because they rely on ideal two-port beam-splitters to construct a Mach-Zhender interferometer. Such beam-splitters cannot be constructed, at least straightforwardly, for nano-crystals as the tunnelling matrix of such massive objects is extremely small  $\propto e^{-\frac{\sqrt{2mV}}{\hbar}\Delta x}$  across any reasonable distance  $\Delta x$  and barrier  $V$ . It is here that our technology of spatial qubit measurements open a way which does not require beam-splitters. We give the upper bound of the position resolution  $\delta x$  in order to verify the entanglement of the spin and motion through a Bell inequality, and show that the system is robust against errors in position detection (as we will clarify, for feasible measurements, the time resolution  $\delta t$  is good enough that it does not lead to errors).

To measure the spin-motion entanglement in the above state, we have to measure variables of spin and spatial qubit. It is convenient to perform the spatial qubit measurement first. As shown in Fig.2, after a required period of free evolution  $t_{\text{meas}}^{x,y}$ , measurements of the spatial qubit operators are made as depicted earlier; the light shone on the object should not interact at all with the embedded spin degree of freedom if it is completely *off-resonant* with any relevant spin transition. Immediately after measuring the spatial qubit, the spin degree of freedom is directly measured in various bases. The latter could be implemented, for example, with a NV centre spin qubit in a nano-diamond crystal, where the spin state is rotated by a microwave pulse, which corresponds to basis change, followed by a fluorescence measurement by shining a laser resonant with an optical transition [62]. As the spin measurement is very

---

<sup>1</sup> Technically, off shell propagation of the mass itself is also involved between the absorption and emmission of photons as depicted

efficient, we only need to consider the resolutions  $\delta x, \delta t$  of the spatial qubit measurements (we integrate over all spreads in the  $y$  and  $z$  directions) so that the effective spatial Pauli  $X$  and  $Y$  operators are then projections onto a mixed state with phase angle ranging from  $\theta - \frac{\delta\theta}{2}$  to  $\theta + \frac{\delta\theta}{2}$  with  $\delta\theta = \frac{md}{\hbar t_{\text{meas}}^{x,y}} \delta x - \frac{xmd}{\hbar (t_{\text{meas}}^{x,y})^2} \delta t$ . For purposes of coherence, which continuously decreases with time, it is best to choose time of the order of the minimum allowed time for overlap of the wavepackets, i.e., choose  $t_{\text{meas}}^{x,y} = d(2\sigma_d m)/\hbar$  so that  $\delta\theta = \frac{\delta x}{2\sigma_d} - \frac{x\hbar}{4\sigma_d^2 md} \delta t$ . The approximate Pauli matrices are then:

$$\begin{aligned}\tilde{\sigma}_x &= \frac{1}{\delta\theta} \begin{pmatrix} 0 & \int_{\theta - \frac{\delta\theta}{2}}^{\theta + \frac{\delta\theta}{2}} e^{-i\theta} d\theta |_{\theta=0} \\ \int_{\theta - \frac{\delta\theta}{2}}^{\theta + \frac{\delta\theta}{2}} e^{i\theta} d\theta |_{\theta=0} & 0 \end{pmatrix} \\ &= \frac{1}{\delta\theta} \begin{pmatrix} 0 & -ie^{i\frac{\delta\theta}{2}} + ie^{-i\frac{\delta\theta}{2}} \\ -ie^{i\frac{\delta\theta}{2}} + ie^{-i\frac{\delta\theta}{2}} & 0 \end{pmatrix}\end{aligned}$$

and similarly,  $\tilde{\sigma}_y = \frac{1}{\delta\theta} \begin{pmatrix} 0 & -e^{i\frac{\delta\theta}{2}} + e^{-i\frac{\delta\theta}{2}} \\ e^{i\frac{\delta\theta}{2}} - e^{-i\frac{\delta\theta}{2}} & 0 \end{pmatrix}$  which reduces to the standard Pauli matrices in the limit  $\delta\theta \rightarrow 0$ . To verify the entanglement we have to show that the spin-motion entangled state violates the Bell-CHSH inequality

$$\mathcal{B} = |\langle AB \rangle + \langle AB' \rangle + \langle A'B \rangle - \langle A'B' \rangle| \leq 2 \quad (5)$$

with variables which maximize the violation of Eq. (5) [63] such as  $A = \tau_x + \tau_y$  and  $A' = \tau_x - \tau_y$  operators of the spin ( $\tau_x$  and  $\tau_y$  are spin Pauli matrices) and  $B = \tilde{\sigma}_x$  and  $B' = \tilde{\sigma}_y$  operators of the spatial qubit.

The expected correlation measures can be calculated (the method of calculating with  $\tilde{\sigma}_x$  and  $\tilde{\sigma}_y$  is given in the appendix) to give:

$$\mathcal{B} = |2\sqrt{2}f(\delta\theta)| \leq 2\sqrt{2} \quad (6)$$

where  $f(\delta\theta) = \frac{2}{\delta\theta} \text{Re}[ie^{i\delta\theta/2}] = \frac{2}{\delta\theta} \cos(\frac{\pi + \delta\theta}{2})$ , and in which the upper bound reduces to  $2\sqrt{2}$  as  $\delta\theta \rightarrow 0$ . To obtain a violation of the CHSH inequality Eq.(5) the upper bound of  $\delta\theta$  can be calculated:  $|f(\delta\theta)| = \frac{1}{\sqrt{2}}$ ,  $\delta\theta \approx 2.783$ . This is approximately 43.7% of  $2\pi$ , which is the resolution required to demonstrate entanglement.

As far as a set of explicit parameters for the problem is concerned, there is a large choice. For example, we consider a  $m \sim 10^{-19}$  kg spin-bearing mass cooled to a ground state in  $\omega \sim 100$  kHz trap (e.g., an optical tweezer [12, 51, 52]) so that its ground state

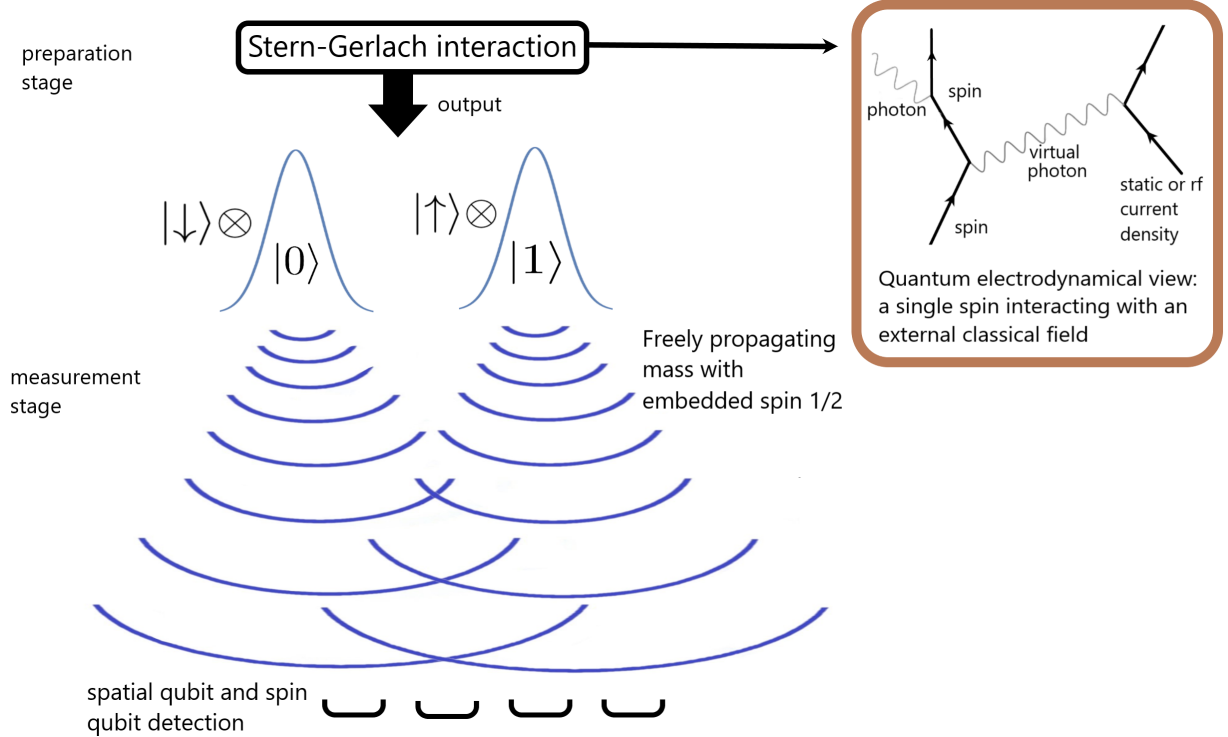


**FIG. 2. Detection scheme for the entanglement of spin and centre of mass of a Stern-Gerlach state:** A spin bearing nano-object is measured to be in a set of zones of size  $\delta x$ , where the size is set by the strength and duration of lasers scattered from the object, which serves to measure the spatial qubit. Within each spatial zone a suitable method is used to measure the spin in different basis, for example by rotating the spin states by microwave pulses followed by fluorescence of certain states under excitation by a laser of appropriate frequency.

spread is  $= \sqrt{\frac{\hbar}{2m\omega}} \sim 1 \text{ \AA}$ . At time  $t = 0$  the embedded spin is placed in a superposition  $1/\sqrt{2}(|\uparrow\rangle + |\downarrow\rangle)$ , and the mass is released from the trap. It is then subject it to an evolution under an inhomogeneous magnetic field gradient  $\sim 10^5 \text{ Tm}^{-1}$  [22]. Due to the Stern-Gerlach effect, the mass moves in opposite directions corresponding to  $|\uparrow\rangle$  and  $|\downarrow\rangle$  spin states, and, in a time-scale of  $t_{\text{prep}} \sim 50 \mu\text{s}$ , evolves to a  $|\phi^+\rangle$  state with a separation of  $d = 25 \text{ nm}$  between the  $|0\rangle$  and  $|1\rangle$  spatial qubit states [19, 22–24, 30] (all lower  $m$  and  $d$  are also possible as they demand lower  $t_{\text{prep}}$  and/or  $\partial B/\partial x$ ). During the above  $t_{\text{prep}}$ , the spreading of the  $|0\rangle$  and  $|1\rangle$  wavepackets is negligible, so that  $\sigma_d \sim 1 \text{ \AA}$ , and  $\sigma_d/d \sim 1/250$ , well within the validity regime of a high fidelity spatial qubit  $\sigma_x$  and  $\sigma_y$  measurement as discussed by us if performed at time  $t_{\text{meas}}^{x,y} \sim \frac{2\sigma_d m d}{\hbar} \sim 1 \text{ ms}$ . According to our results above, in order to obtain

a CHSH inequality violation, one has to measure to within  $\delta x \sim 2\sigma_d \delta\theta \sim 1 \text{ \AA}$  resolution. This is possible as there are feasible techniques that give resolutions of  $0.1 \text{ pm}/\sqrt{\text{Hz}}$  [57, 58] for position measurements by scattering light continuously from an object. In fact, we would need to scatter light only for a  $\mu\text{s}$  to achieve our required resolution. On the other hand if the timing accuracy  $\delta t$  of  $t_{\text{meas}}^{x,y}$  is kept below  $\sim 0.1\text{ms}$  (also easy in terms of laser switching on/off times), there is a negligible inaccuracy in  $\theta$ .

Note that as shown in the appendix, dephasing between the spatial states  $|0\rangle$  and  $|1\rangle$  at a rate  $\gamma$  simply suppresses the CHSH violation by a factor  $e^{-\gamma t}$ , which could be a new way to investigate decoherence of the mass from various postulated collapse models [13–18], as well as from standard environment. As *both* the ancillary spin and the mass are measured, it characterizes the entanglement of the given state (a kinematic feature – a feature of Hilbert space states alone) *irrespective* of the dynamics (the Hamiltonian and initial state) from which the state was generated, as opposed to many of the previous protocols which rely crucially on a reversible nature of the quantum dynamics leading to periodic entanglement and disentanglement of an ancillary system and a mass [5–8]. As opposed to single object interferometry [12, 53, 54], in which one targets a specific basis to examine decoherence, here the CHSH violation explores the decoherence of the mass in multiple bases. For example, we will not only learn how the off diagonal terms  $|0\rangle\langle 1|$  of the spatial qubit decay (position basis decoherence), we will also learn whether, and, if so, how,  $|+\rangle\langle -|$  decays (where  $|-\rangle = |0\rangle - |1\rangle$ ) – this would be equivalent to identifying a novel type of decoherence of superpositions of even and odd parity states. Moreover, as the total spin-motional system is quantum 4 state system, and, as was shown in Refs.[31, 32], the above CHSH violation can also be regarded as a test of quantum violation of the classical notion of non-contextuality, which is yet to be tested for macroscopic masses.

*Casimir induced entanglement:* Neutral unmagnetized masses that do not interact significantly with voltage/current/magnetic noise, and are free in the sense of not interacting with any external field (to control it or to trap it, for example) are ideal for the preservation of spatial coherence. To entangle two such masses, we need a suitable interaction. A means by which they can strongly (by which here we mean electromagnetically) interact with other neutral masses is the Casimir interaction (gravity becomes significant enough to cause observable effects on a reasonable time-scale only for masses  $> 10^{-15} - 10^{-14} \text{ kg}$ , and may require sufficiently separated masses [19] or the Casimir force to be screened [23]).

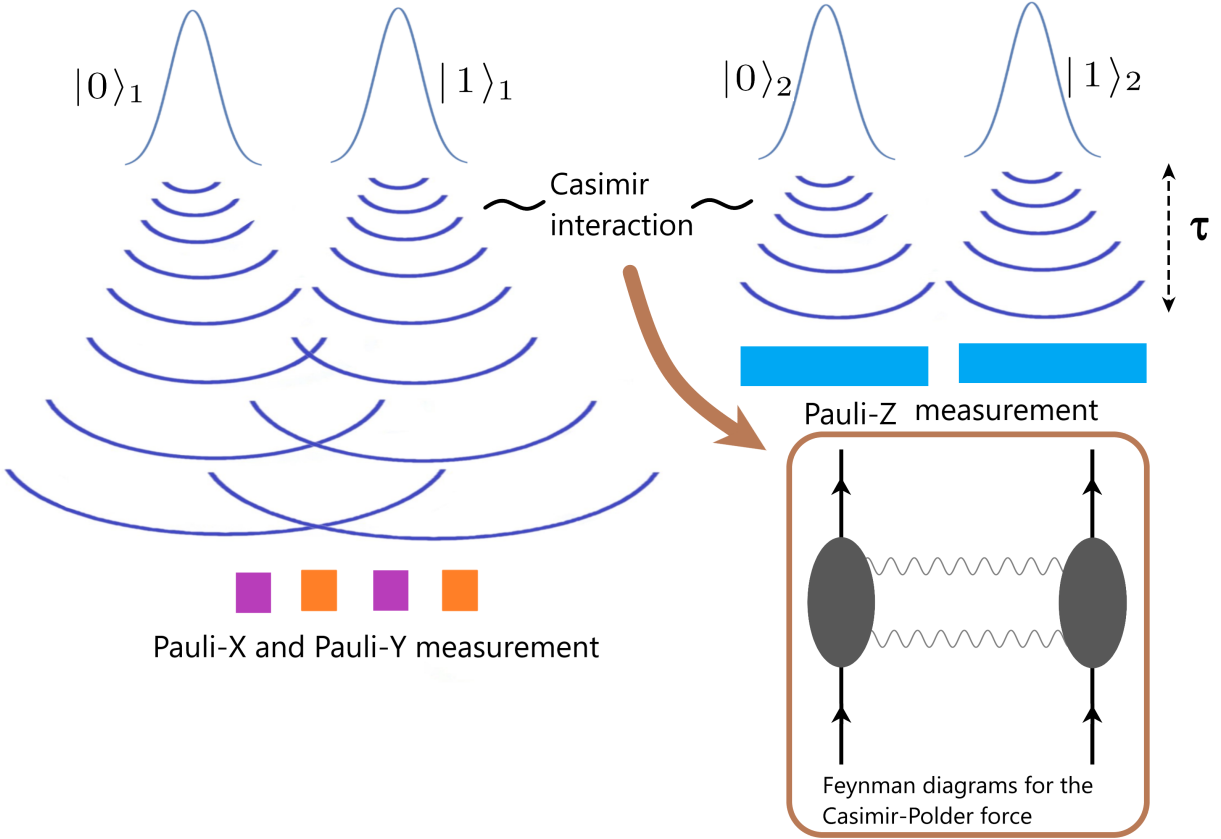


**FIG. 3. Application in entanglement witnessing of two masses:** Two masses, each prepared in a superposition of two states, act as two qubits  $\frac{1}{\sqrt{2}}(|0\rangle_1 + |1\rangle_1) \otimes \frac{1}{\sqrt{2}}(|0\rangle_2 + |1\rangle_2)$ . The system freely propagates and undergoes mutual interactions for a time  $\tau$ . This interaction induces entanglement which can be deduced from spatial qubit Pauli measurements. To evaluate the entanglement witness  $W$ , we conduct spatial qubit measurements on both masses and evaluate the correlations. For example, in the figure, Pauli-X, Pauli-Y measurements on test mass 1 and Pauli-Z measurements on test mass 2 are depicted. Casimir interaction, is shown, and will have virtual photons as the quantum mediators [64].

In this section, we show how to generate entanglement using the Casimir interaction and witness it using our spatial qubit methodology with just the cost of applying an *additional squeezing* operator to the spatial qubit states before the  $\sigma_x, \sigma_y$  measurements. The nature of the entanglement between two spatial qubits is highly non-Gaussian in nature. As shown in Fig 3, two neutral test masses (mass  $m$ ) indexed 1 and 2, each prepared in the spatial qubit state  $|+\rangle$ . The superposition size (separation between states  $|0\rangle$  and  $|1\rangle$ ) is  $d$ , the radius of the masses is  $R$ , while the distance between the centres of the superpositions is  $D$ .

The system evolves for a time  $\tau$  due to the Casimir interaction and gets entangled as the interactions induce a relative phase between different components of the superposition due to different separation distances. The evolution of the system is then given by [19]:

$$\begin{aligned} |\psi(t=0)\rangle &= \frac{1}{\sqrt{2}}(|0\rangle_1 + |1\rangle_1) \frac{1}{\sqrt{2}}(|0\rangle_2 + |1\rangle_2) \\ \rightarrow |\psi(t=\tau)\rangle &= \frac{e^{i\phi}}{\sqrt{2}}[|0\rangle_1 \frac{1}{\sqrt{2}}(|0\rangle_2 + e^{i\Delta\phi_{01}}|1\rangle_2) \\ &\quad + |1\rangle_1 \frac{1}{\sqrt{2}}(e^{i\Delta\phi_{10}}|0\rangle_2 + |1\rangle_2)] \end{aligned} \quad (7)$$

where  $\phi, \Delta\phi_{01}, \Delta\phi_{10}$  are induced relative phases. For example, for the Casimir-Polder interaction, the relevant phases are:  $\phi = k \frac{R^6}{D^7} t, \Delta\phi_{01} = k \frac{R^6}{(D+d)^7} t - \phi, \Delta\phi_{10} = k \frac{R^6}{(D-d)^7} t - \phi$ , where  $k = \frac{23c}{4\pi}(\epsilon - 1)^2/(\epsilon + 2)^2$ , where  $\epsilon$  is the relative permittivity of the material of the masses. On top of the above evolution, we assume a local dephasing of the spatially separated off diagonal terms  $|0\rangle\langle 1|_i \rightarrow e^{-\gamma\tau}|0\rangle\langle 1|_i$  for both particles ( $i = 1, 2$ ) during the time  $\tau$  (this can generically take into account all dephasing effects [23, 65]). To verify the induced entanglement, *after* the interaction time  $\tau$ , one can make spatial qubit measurements up to uncertainties  $\delta x, \delta t$  parametrized by  $\delta\theta$  as outlined previously and then estimate the entanglement witness [66]  $W = I \otimes I - \tilde{\sigma}_x \otimes \tilde{\sigma}_x - \tilde{\sigma}_z \otimes \tilde{\sigma}_y - \tilde{\sigma}_y \otimes \tilde{\sigma}_z$  (schematic diagram shown in Fig.3), where  $\tilde{\sigma}_x$  and  $\tilde{\sigma}_y$  are as discussed before, and we take  $\tilde{\sigma}_z = \int_{-\infty}^0 |x\rangle\langle x| dx - \int_0^\infty |x\rangle\langle x| dx$ , as for example, used in Ref.[67]. If  $\langle W \rangle = Tr(W\rho)$  is negative, the masses are entangled. As a technical point, note here that the form of witness operator compels one to measure both the  $\tilde{\sigma}_x \otimes \tilde{\sigma}_x$  operator and the other two operators on the *same entangled state*. Thus we require  $t_{\text{meas}}^{x,y} - t_{\text{meas}}^z \ll \tau$  so that the extra entanglement generated due to interactions after the  $\tilde{\sigma}_z$  measurement and before the  $\tilde{\sigma}_x/\tilde{\sigma}_y$  measurements is negligible. This, in turn, requires us to *speed up* the development of spatial overlap between the qubit states due to wavepacket spreading after the  $\tilde{\sigma}_z$  measurement, which can be accomplished by squeezing both of the wavepackets in position after the time  $t_{\text{meas}}^z$ . This squeezing, on the other hand, can be accomplished unitarily by making the masses pass through local Harmonic potentials in the  $x$  direction with frequency modulation. For example  $n$  repeated changes between  $\omega_1$  and  $\omega_2$  separated by appropriate periods of harmonic evolution will squeeze by the factor  $(\omega_1/\omega_2)^n$  [68] as long as any extra decoherence induced by the very application of the harmonic potential is  $\gamma_{\text{squeeze}} \ll (n/\omega_1 + n/\omega_2)^{-1}$ .

Assuming uncertainties  $\delta\theta$  in placement, and a decoherence rate  $\gamma$  for the masses, the

expectation value of the witness operator is

$$\begin{aligned}\langle \tilde{W} \rangle = & 1 - \frac{1}{2} e^{-2\gamma t} g^2(\delta\theta) (1 + \cos(\Delta\phi_{10} - \Delta\phi_{01})) \\ & - e^{-\gamma t} g(\delta\theta) (\sin(\Delta\phi_{10}) + \sin(\Delta\phi_{01})),\end{aligned}\quad (8)$$

where  $g(\delta\theta) = \frac{2}{\delta\theta} \cos(\frac{\pi - \delta\theta}{2})$ . As Eq.(8) can yield the witness for any finite decoherence and systematic uncertainties, we will concentrate here on the ideal case ( $\gamma \ll 1/\tau, 1/t_{\text{meas}}^z, 1/t_{\text{meas}}^{x,y}$  and  $\delta\theta \sim 0$ ) to highlight the parameter regimes in which to evidence Casimir/Newtonian entanglement.

We are going to consider the Stern-Gerlach mechanism, just as in the previous application, to first prepare the state  $|\phi^+\rangle$ , and from that use the mechanisms of either Refs.[28, 29] or Ref.[54] to prepare  $|+\rangle$ . We consider a  $R \sim 20$  nm,  $m \sim 10^{-19}$  kg mass, and consider it to have been trapped and cooled it to its ground state ( $\sigma_d \sim 1$  nm) in a 1 kHz trap (as envisaged in [54]). We then release it, and subject it to a magnetic field gradient of  $5 \times 10^4$  Tm<sup>-1</sup> [22] for  $t \sim 100\mu\text{s}$  so that a Stern-Gerlach splitting of  $d \approx 50$  nm develops while there is insignificant wavepacket splitting ( $\sigma_d$  remains  $\sim 1$  nm). At this stage, a microwave pulse may be given to rotate the spin state so that the  $|\phi^+\rangle$  state evolves to  $|0\rangle(|\uparrow\rangle + |\downarrow\rangle) + |1\rangle(|\uparrow\rangle - |\downarrow\rangle)$ . A subselection of the  $|\uparrow\rangle$  spin state as in Refs.[28, 29], via deflection through another Stern-Gerlach, for example, yields the state  $|+\rangle$ . Alternatively, by performing a conditional gate (essentially a CNOT) with the spatial qubit as the control and the spin as the target (again, performed quite accurately by a microwave pulse as described in Ref.[54]),  $|\phi^+\rangle$  gets converted to  $|+\rangle|\downarrow\rangle$  so that the spatial part is our required state. If we assume  $D \approx 3.5\mu\text{m}$ , then  $\Delta\phi_{RL} = \phi_{RL} - \phi \approx 0.036$ ,  $\Delta\phi_{LR} = \phi_{LR} - \phi \approx -0.032$  after  $\tau \sim 0.01\text{s}$  of entangling time, which gives a negative witness  $\langle W \rangle \sim -0.00287$ .  $\tilde{\sigma}_z$  measurement is also done at  $t_{\text{meas}}^z = \tau$ . This is about 0.1 of the overlapping time  $\sim \frac{d(2\sigma_d m)}{\hbar}$  so that the fidelity of the  $\sigma_z$  measurement is very high (see appendix). However, we require to conduct the  $XY$  measurement as soon as possible after the  $z$  measurement as mentioned above, in order to prevent further growth of entanglement. After 0.01 s of flight, the wavepacket width  $\sigma_d \sim 1$  nm expands to  $\sim 10$  nm. Then, we squeeze the state by 2 orders of magnitude to  $\sim 1 \times 10^{-10}$  m, so that it expands to  $\sim 100$  nm, where overlapping occurs, in the next 0.001s. The fidelity of  $XY$  measurement here is very high (see appendix). The slight delay in Pauli-X,Y measurement (0.001s later than the Pauli-Z measurement) would cause only a  $\sim 5\%$  error in the witness magnitude. Note that in order to achieve the required squeezing, two appropriate periods

of evolution in harmonic potentials of  $\omega_1 \sim 1$  MHz and  $\omega_2 \sim 0.1$  MHz would suffice; if this potential was applied as an optical tweezer then it will hardly cause any decoherence  $\gamma_{\text{squeeze},j} \sim \omega_j 10^{-5}$  [9]. This entanglement by the Casimir interaction could be one of the earliest demonstrations of non-Gaussian entanglement between two masses. It would also provide a route to demonstrate the nonclassical nature of the Casimir interaction, namely that it is mediated by quantum agents (virtual photons) as depicted in the inset of Fig.3.

*Conclusions:* We have shown how to measure spatial qubit operators  $\sigma_x, \sigma_y$  and  $\sigma_z$  of a massive object by the free evolution, resulting interference and position measurement. We have then applied this methodology to the following fundamentally important applications: (a) testing the validity of quantum physics for the centre of mass of objects much more massive than macromolecules (nano-crystals to be precise) – here we show how aspects such as quantum contextuality, never before tested for macroscopic objects, can be evidenced, (b) preparing two-qubit entanglement between spatial states of two such objects, again extending the boundaries of quantum technology to a more macroscopic scale, (c) probing the quantum coherent nature of the Casimir force – while it is theoretically known that the Casimir interaction has a quantum origin, an experimental proof is still lacking. Indeed, in the *same* open-minded way that one asks whether quantum mechanics continues to remain for macroscopic masses [1, 2], one can ask the question as to whether those interactions between such masses which are extensive in nature (grow as volume/area/mass) *continue* to remain quantum in the sense of being mediated by a quantum natured field so as to be able to entangle the masses. For example, one could argue that perhaps there is a regime in which, although individual masses are quantum, they do not entangle as the interactions between them are classical – experiments to date with large masses have not been able to discount such a possibility. In comparison with standard approaches for probing the nonclassicality for smaller masses, we avoid a complete Mach-Zehnder type interferometer – only requiring the preparation of an original spatial superposition, and a subsequent free evolution. This is advantageous because of the difficulty of realizing beam-splitters using nano-objects due to the tunneling probability getting smaller for larger masses, and also for avoiding interactions with mirrors and beam splitters which can cause decoherence. Essentially the two-slit experiment is itself a beam-splitter [69] (see appendix), which is being exploited here. Our methodology is particularly robust against imprecision in spatial detection. Obviously this can also open up several applications in the sense that it enables

the plethora of qubit based quantum protocols to be adapted to untrapped masses with continuous degrees of freedom.

## ACKNOWLEDGMENTS

DH and US would like to acknowledge partial support from the DST-ITPAR grant IMT/Italy/ITPAR-IV/QP/2018/G. DH also acknowledges support from the NSAI Senior Scientist fellowship. AM's research is funded by the Netherlands Organisation for Science and Research (NWO) grant number 680-91-119. SB would like to acknowledge EPSRC Grant Nos. EP/N031105/1 and EP/S000267/1.

---

- [1] A. J. Leggett, *Journal of Physics: Condensed Matter* **14**, R415 (2002).
- [2] M. Arndt, K. Hornberger, and A. Zeilinger, *Physics world* **18**, 35 (2005).
- [3] S. Gerlich, S. Eibenberger, M. Tomandl, S. Nimmrichter, K. Hornberger, P. J. Fagan, J. Tüxen, M. Mayor, and M. Arndt, *Nature communications* **2**, 1 (2011).
- [4] Y. Y. Fein, P. Geyer, P. Zwick, F. Kiałka, S. Pedalino, M. Mayor, S. Gerlich, and M. Arndt, *Nature Physics* **15**, 1242 (2019).
- [5] S. Bose, K. Jacobs, and P. L. Knight, *Physical Review A* **59**, 3204 (1999).
- [6] A. Armour, M. Blencowe, and K. C. Schwab, *Physical Review Letters* **88**, 148301 (2002).
- [7] W. Marshall, C. Simon, R. Penrose, and D. Bouwmeester, *Physical Review Letters* **91**, 130401 (2003).
- [8] S. Bose, *Physical review letters* **96**, 060402 (2006).
- [9] D. E. Chang, C. Regal, S. Papp, D. Wilson, J. Ye, O. Painter, H. J. Kimble, and P. Zoller, *Proceedings of the National Academy of Sciences* **107**, 1005 (2010).
- [10] O. Romero-Isart, M. L. Juan, R. Quidant, and J. I. Cirac, *New Journal of Physics* **12**, 033015 (2010).
- [11] O. Romero-Isart, A. C. Pflanzer, F. Blaser, R. Kaltenbaek, N. Kiesel, M. Aspelmeyer, and J. I. Cirac, *Physical review letters* **107**, 020405 (2011).
- [12] O. Romero-Isart, *Physical Review A* **84**, 052121 (2011).
- [13] L. Diósi, *Physical Review A* **40**, 1165 (1989).

- [14] R. Penrose, General relativity and gravitation **28**, 581 (1996).
- [15] A. Bassi, K. Lochan, S. Satin, T. P. Singh, and H. Ulbricht, Reviews of Modern Physics **85**, 471 (2013).
- [16] G. Milburn, Physical Review A **44**, 5401 (1991).
- [17] J. Oppenheim, arXiv preprint arXiv:1811.03116 (2018).
- [18] S. Weinberg, Phys. Rev. A **85**, 062116 (2012).
- [19] S. Bose, A. Mazumdar, G. W. Morley, H. Ulbricht, M. Toroš, M. Paternostro, A. A. Geraci, P. F. Barker, M. Kim, and G. Milburn, Physical review letters **119**, 240401 (2017).
- [20] R. J. Marshman, A. Mazumdar, and S. Bose, Physical Review A **101**, 052110 (2020).
- [21] C. Marletto and V. Vedral, Physical review letters **119**, 240402 (2017).
- [22] Y. Margalit, O. Dobkowski, Z. Zhou, O. Amit, Y. Japha, S. Moukouri, D. Rohrlich, A. Mazumdar, S. Bose, C. Henkel, *et al.*, arXiv preprint arXiv:2011.10928 (2020).
- [23] T. W. van de Kamp, R. J. Marshman, S. Bose, and A. Mazumdar, Physical Review A **102**, 062807 (2020).
- [24] R. J. Marshman, A. Mazumdar, G. W. Morley, P. F. Barker, S. Hoekstra, and S. Bose, New Journal of Physics **22**, 083012 (2020).
- [25] B. Englert, J. Schwinger, and M. Scully, Found Phys **18**, 1045 (1988).
- [26] D. Home, A. K. Pan, M. M. Ali, and A. Majumdar, Journal of Physics A: Mathematical and Theoretical **40**, 13975 (2007).
- [27] M. Keil, S. Machluf, Y. Margalit, Z. Zhou, O. Amit, O. Dobkowski, Y. Japha, S. Moukouri, D. Rohrlich, Z. Binstock, *et al.*, arXiv preprint arXiv:2009.08112 (2020).
- [28] Y. Margalit, Z. Zhou, S. Machluf, Y. Japha, S. Moukouri, and R. Folman, New Journal of Physics **21**, 073040 (2019).
- [29] S. Machluf, Y. Japha, and R. Folman, Nature Communications **4**, 2424 (2013).
- [30] C. Wan, M. Scala, G. Morley, A. A. Rahman, H. Ulbricht, J. Bateman, P. Barker, S. Bose, and M. Kim, Physical review letters **117**, 143003 (2016).
- [31] S. Basu, S. Bandyopadhyay, G. Kar, and D. Home, Physics Letters A **279**, 281 (2001).
- [32] D. Home and S. Sengupta, Physics Letters A **102**, 159 (1984).
- [33] C. Pfister, J. Kaniewski, M. Tomamichel, A. Mantri, R. Schmucker, N. McMahon, G. Milburn, and S. Wehner, Nature communications **7**, 1 (2016).
- [34] D. Kafri and J. Taylor, arXiv preprint arXiv:1311.4558 (2013).

[35] T. Krisnanda, M. Zuppardo, M. Paternostro, and T. Paterek, *Physical review letters* **119**, 120402 (2017).

[36] S. Osnaghi, P. Bertet, A. Auffeves, P. Maioli, M. Brune, J.-M. Raimond, and S. Haroche, *Physical Review Letters* **87**, 037902 (2001).

[37] A. J. Landig, J. V. Koski, P. Scarlino, C. Müller, J. C. Abadillo-Uriel, B. Kratochwil, C. Reichl, W. Wegscheider, S. N. Coppersmith, M. Friesen, *et al.*, *Nature communications* **10**, 1 (2019).

[38] S. K. Lamoreaux, *Annual Review of Nuclear and Particle Science* **62**, 37 (2012).

[39] Z. Xu and T. Li, *Physical Review A* **96**, 033843 (2017).

[40] Z. Xu, X. Gao, J. Bang, Z. Jacob, and T. Li, *arXiv preprint arXiv:2102.12857* (2021).

[41] S. Qvarfort, S. Bose, and A. Serafini, *Journal of Physics B: Atomic, Molecular and Optical Physics* **53**, 235501 (2020).

[42] T. Krisnanda, G. Y. Tham, M. Paternostro, and T. Paterek, *npj Quantum Information* **6**, 1 (2020).

[43] T. Weiss, M. Roda-Llordes, E. Torrontegui, M. Aspelmeyer, and O. Romero-Isart, *arXiv preprint arXiv:2012.12260* (2020).

[44] R. Simon, *Physical Review Letters* **84**, 2726 (2000).

[45] G. Taguchi, T. Dougakiuchi, N. Yoshimoto, K. Kasai, M. Iinuma, H. F. Hofmann, and Y. Kadoya, *Physical Review A* **78**, 012307 (2008).

[46] D. Ghosh, T. Jennewein, P. Kolenderski, and U. Sinha, *OSA Continuum* **1**, 996 (2018).

[47] R. Sawant, J. Samuel, A. Sinha, S. Sinha, and U. Sinha, *Physical review letters* **113**, 120406 (2014).

[48] P. Kolenderski, U. Sinha, L. Youning, T. Zhao, M. Volpini, A. Cabello, R. Laflamme, and T. Jennewein, *Physical Review A* **86**, 012321 (2012).

[49] G. Rengaraj, U. Prathwiraj, S. N. Sahoo, R. Somashekhar, and U. Sinha, *New Journal of Physics* **20**, 063049 (2018).

[50] P. Barker and M. Shneider, *Physical Review A* **81**, 023826 (2010).

[51] U. Delić, M. Reisenbauer, K. Dare, D. Grass, V. Vuletić, N. Kiesel, and M. Aspelmeyer, *Science* **367**, 892 (2020).

[52] F. Tebbenjohanns, M. Frimmer, A. Militaru, V. Jain, and L. Novotny, *Physical review letters* **122**, 223601 (2019).

[53] J. Bateman, S. Nimmrichter, K. Hornberger, and H. Ulbricht, *Nature communications* **5**, 1 (2014).

[54] Z.-q. Yin, T. Li, X. Zhang, and L. Duan, *Physical Review A* **88**, 033614 (2013).

[55] M. Scala, M. Kim, G. Morley, P. Barker, and S. Bose, *Physical review letters* **111**, 180403 (2013).

[56] D. Gottesman, A. Kitaev, and J. Preskill, *Physical Review A* **64**, 012310 (2001).

[57] J. Gieseler, B. Deutscher, R. Quidant, and L. Novotny, *Phys. Rev. Lett.* **109**, 103603 (2012).

[58] J. Vovrosh, M. Rashid, D. Hempston, J. Bateman, M. Paternostro, and H. Ulbricht, *JOSA B* **34**, 1421 (2017).

[59] A. Lvovsky, R. Ghobadi, A. Chandra, A. Prasad, and C. Simon, *Nature Physics* **9**, 541 (2013).

[60] A. Tiranov, J. Lavoie, P. C. Strassmann, N. Sangouard, M. Afzelius, F. Bussières, and N. Gisin, *Physical review letters* **116**, 190502 (2016).

[61] Y. Hasegawa, R. Loidl, G. Badurek, M. Baron, and H. Rauch, *Phys. Rev. Lett.* **97**, 230401 (2006).

[62] B. Hensen, H. Bernien, A. E. Dréau, A. Reiserer, N. Kalb, M. S. Blok, J. Ruitenberg, R. F. Vermeulen, R. N. Schouten, C. Abellán, *et al.*, *Nature* **526**, 682 (2015).

[63] J. F. Clauser, M. A. Horne, A. Shimony, and R. A. Holt, *Phys. Rev. Lett.* **24**, 549 (1970).

[64] G. Feinberg and J. Sucher, *Physical Review A* **2**, 2395 (1970).

[65] M. Toroš, T. W. van de Kamp, R. J. Marshman, M. Kim, A. Mazumdar, and S. Bose, arXiv preprint arXiv:2007.15029 (2020).

[66] H. Chevalier, A. J. Paige, and M. S. Kim, *Phys. Rev. A* **102**, 022428 (2020).

[67] S. Bose, D. Home, and S. Mal, *Physical review letters* **120**, 210402 (2018).

[68] T. Kiss, P. Adam, and J. Janszky, *Physics Letters A* **192**, 311 (1994).

[69] S. Sadana, B. C. Sanders, and U. Sinha, *New Journal of Physics* **21**, 113022 (2019).

## Appendix A: Efficacy of the Pauli-Z measurement as a function of measurement time

The system freely propagates for a time  $t$ , the final state may be written, for an initial state  $|+\rangle$ , as:

$$\langle x|\Psi(t)\rangle = \frac{1}{[2\pi\sigma^2]^{1/4}} \sqrt{\frac{1}{\frac{1}{s} - i\frac{\hbar t}{2m}}} \times \left\{ \exp\left[-\frac{(x - \frac{d}{2\sigma_d^2 s})^2}{4(\frac{1}{s} - i\frac{\hbar t}{2m})}\right] + \exp\left[-\frac{(x + \frac{d}{2\sigma_d^2 s})^2}{4(\frac{1}{s} - i\frac{\hbar t}{2m})}\right] \right\} \quad (\text{A1})$$

where  $s \equiv \frac{i4\phi}{\sigma^2} + \frac{1}{\sigma^2} + \frac{1}{\sigma_d^2}$ ,  $\phi$  is global phase added during the propagation.

Note that Eq.A1 consists of two terms tracing which path the object passes through, effectively the predefined Young qubit.  $\sigma_z$  measurement requires that the wave packets are well separated upon measurement. The condition maybe formulated by demanding the probability distribution  $P_0$  ( $P_1$ ) of  $|0\rangle$  ( $|1\rangle$ ) state alone confined in the  $x < 0$  ( $x > 0$ ) regime:

$$\epsilon = 1 - \frac{\int_{-\infty}^0 P_0 dx}{\int_{-\infty}^{\infty} P_0 dx} \ll 1 \quad (\text{A2})$$

Substituting eqA1, the fraction term can be evaluated at the  $\sigma_z$  measurement time  $t = t_{\text{meas}}^z$ :

$$\frac{\int_{-\infty}^0 P_0 dx}{\int_{-\infty}^{\infty} P_0 dx} = \frac{\int_{-\infty}^0 \exp\left[-\frac{(x + \frac{d}{2\sigma_d^2 s})^2 \frac{1}{s}}{\frac{2}{s^2} + \frac{\hbar^2 t^2}{8m^2}}\right] dx}{\int_{-\infty}^{\infty} \exp\left[-\frac{(x + \frac{d}{2\sigma_d^2 s})^2 \frac{1}{s}}{\frac{2}{s^2} + \frac{\hbar^2 t^2}{8m^2}}\right] dx} \quad (\text{A3})$$

where the normalization factor in the probability distribution, independent of  $x$ , cancels out in the calculation.

Let us take  $\sigma_d : d = 1 : 50$  and  $t_{\text{meas}}^z \approx$  one-tenth of the overlapping time  $\frac{d(2\sigma_d m)}{\hbar}$ . We then get  $\epsilon \sim (1 - 4.7 \times 10^{-7})$ . We may thus claim that for the above choice of parameters the left and right Gaussian wavepackets are well separated, and Pauli-Z measurement has a good fidelity.

## Appendix B: Efficacy of the Pauli-X and Pauli-Z measurement for various parameters

We take  $t = t_{\text{meas}}^{x,y} \sim \frac{2\sigma_d m d}{\hbar}$  as the time of  $\sigma_x$ ,  $\sigma_y$  measurement, and evaluate how accurate this measurement is for various ratios  $\sigma_d : d$  using the full time evolution as in A1. Our

target is to check how accurately the interference pattern is reproduced at correct positions as given by  $x = \frac{\hbar k_x t_{\text{meas}}^{x,y}}{m}$ . For an initial state  $|0\rangle + |1\rangle$ , if  $\sigma_d : d = 1 : 10$  the first peak of the interference pattern adjacent to the central peak (corresponding to  $\theta = 2\pi$ ) locates at  $x \sim 11.797\sigma_d$ . If  $\sigma_d : d = 1 : 100$ ,  $x \sim 12.559\sigma_d$ . If  $\sigma_d : d = 1 : 50$ ,  $x \sim 12.536\sigma_d$ . While assumption  $x = \frac{\hbar k_x t_{\text{meas}}^{x,y}}{m}$  gives a value of  $x = 4\pi\sigma_d \sim 12.566\sigma_d$ , which is  $>\sim 99.94\%$  accurate for  $\frac{\sigma_d}{d} \leq \frac{1}{100}$ ,  $>\sim 99.76\%$  accurate for  $\frac{\sigma_d}{d} \leq \frac{1}{50}$ . Therefore, the  $\sigma_x$ ,  $\sigma_y$  measurements have a good fidelity in the  $\frac{\sigma_d}{d} \leq \frac{1}{50}$  setting, which we shall use.

### Appendix C: Methods of computation with effective Pauli operators including uncertainties, and the incorporation of decoherence

Let  $\tilde{\sigma}$  denotes the measured Pauli operator, parameterized by uncertainty in phase angle  $\delta\theta$ . Then,

$$\begin{aligned}\tilde{\sigma}_x &= \frac{1}{\delta\theta} \begin{pmatrix} 0 & -ie^{i\frac{\delta\theta}{2}} + ie^{-i\frac{\delta\theta}{2}} \\ -ie^{i\frac{\delta\theta}{2}} + ie^{-i\frac{\delta\theta}{2}} & 0 \end{pmatrix} \\ &= g(\delta\theta)\sigma_x\end{aligned}\quad (\text{C1})$$

where  $g(\delta\theta) = -ie^{i\frac{\delta\theta}{2}} + ie^{-i\frac{\delta\theta}{2}} = \frac{2}{\delta\theta} \cos\left(\frac{\pi - \delta\theta}{2}\right)$ .  $g(\delta\theta)$  goes to 1 as  $\delta\theta \rightarrow 0$ . Similarly,

$$\tilde{\sigma}_y = g(\delta\theta)\sigma_y \quad (\text{C2})$$

Therefore, for arbitrary density state  $\rho$

$$\text{Tr}(\tilde{\sigma}_x \rho) = g(\delta\theta) \text{Tr}(\sigma_x \rho) \quad (\text{C3})$$

$$\text{Tr}(\tilde{\sigma}_y \rho) = g(\delta\theta) \text{Tr}(\sigma_y \rho)$$

In particular, let  $\rho_{x+}$  ( $\rho_{y+}$ ) denotes the positive eigenstate of  $\sigma_x$  ( $\sigma_y$ ), and  $\rho_{x+} = \frac{1}{2} \begin{pmatrix} 1 & 1 \\ 1 & 1 \end{pmatrix}$ ,  $\rho_{y+} = \frac{1}{2} \begin{pmatrix} 1 & -i \\ i & 1 \end{pmatrix}$ . Then,

$$\text{Tr}(\tilde{\sigma}_x \rho_{x+}) = \text{Tr}(\tilde{\sigma}_y \rho_{y+}) = g(\delta\theta) \quad (\text{C4})$$

Furthermore, if decoherence is considered, let  $\tilde{\rho} = \begin{pmatrix} \rho_{00} & \rho_{01}e^{-\gamma t} \\ \rho_{10}e^{-\gamma t} & \rho_{11} \end{pmatrix}$ , where  $\gamma$  denotes dephasing rate, then we have:

$$\text{Tr}(\tilde{\sigma}_x \tilde{\rho}) = g(\delta\theta) \text{Tr}(\sigma_x \rho) e^{-\gamma t} \quad (\text{C5})$$

$$\text{Tr}(\tilde{\sigma}_y \tilde{\rho}) = g(\delta\theta) \text{Tr}(\sigma_y \rho) e^{-\gamma t}$$

## Appendix D: Decoherence in probing the entanglement of the Stern-Gerlach state

Consider the state  $\phi^+ = \frac{1}{\sqrt{2}}(|\uparrow, R\rangle + |\downarrow, L\rangle)$ , where the spatial qubit undergoes decoherence. The density state can be written as

$$\tilde{\rho}(\phi^+) = \frac{1}{2} \begin{pmatrix} 0 & 0 & 0 & 0 \\ 0 & 1 & e^{-\gamma t} & 0 \\ 0 & e^{-\gamma t} & 1 & 0 \\ 0 & 0 & 0 & 0 \end{pmatrix} \quad (\text{D1})$$

$$\text{Tr}(\sigma_x \otimes \sigma_x \tilde{\rho}(\phi^+)) = \text{Tr}(\sigma_y \otimes \sigma_y \tilde{\rho}(\phi^+)) = e^{-\gamma t} \quad (\text{D2})$$

$$\text{Tr}(\sigma_x \otimes \sigma_y \tilde{\rho}(\phi^+)) = \text{Tr}(\sigma_y \otimes \sigma_x \tilde{\rho}(\phi^+)) = 0$$

Therefore,

$$|\langle ab \rangle + \langle ab' \rangle + \langle a'b \rangle - \langle a'b' \rangle| = |2\sqrt{2}g(\delta\theta)e^{-\gamma t}| \leq 2\sqrt{2} \quad (\text{D3})$$

## Appendix E: Young type qubit as beam splitter

Our experimental setup serves the same purpose as a Mach-Zehnder interferometer in probing contextuality[31], in which a particle pass through beam splitters and which path information defines a spatial qubit. In our approach, Young type double slit acts effectively as a lossy beam splitter [69]. A cubic beam splitter has two input and two output. The transformation matrix from the former to the latter ports is described by a two-by-two unitary matrix. The initial states  $|0\rangle$  and  $|1\rangle$  act as the two input. By placing a pair of detectors in the interference plane, we project the input states onto a different basis, parameterized by phase angle  $\theta$ . For instance, conducting Pauli-y operation requires placing two detectors at phase angle  $-\pi/2$  and  $\pi/2$  respectively. The effective beam splitter therefore transforms the system from a superposition of  $|0\rangle$  and  $|1\rangle$  to the basis spanned by  $|0\rangle - i|1\rangle$  and  $|0\rangle + i|1\rangle$ . The transformation matrix is therefore  $\frac{1}{\sqrt{2}} \begin{pmatrix} 1 & i \\ 1 & -i \end{pmatrix} = \frac{1}{\sqrt{2}} \begin{pmatrix} 1 & i \\ i \times e^{-i\pi/2} & 1 \times e^{-i\pi/2} \end{pmatrix}$ , equivalently, a 50:50 beam splitter followed by a phase shifter with angle  $-\pi/2$ .